RSC Advances

ROYAL SOCIETY OF CHEMISTRY

www.rsc.org/advances

Riboflavin detection by α–Fe_2O_3/MWCNT/AuNPs-based composite and study of the interaction of riboflavin with DNA

C.Sumathi [a], P.Muthukumaran [a], S.Radhakrishnan[b] , G.Ravi [c] , J.Wilson [a*]

[a]Polymer Electronics Lab, Department of Bioelectronics and Biosensors, Alagappa University, Karaikudi-630003, Tamilnadu, India

[b] Nanomaterials and System Lab, Department of Mechanical System Engineering, Jeju National University, Jeju 690-756, Republic of Korea

[c] Photonic Crystals Lab, Department of physics, Alagappa University, Karaikudi-630003, Tamilnadu, India

*Corresponding Author:

Dr. J. Wilson

E-mail: wilson.j2008@yahoo.com

List of Abbreviations

RF– riboflavin

CV– cyclic voltammetry

SWV – square wave voltammetry

ds-DNA – double stranded deoxy ribonucleic acid

RF-ds-DNA – riboflavin - double stranded deoxy ribonucleic acid

RSD – relative standard deviation

FMN – flavin mononucleotide

FAD – flavin adenine dinucleotide

UV radiation exposure – Ultra violet radiation exposure

CNT – carbon nanotubes

AuNPs – gold nanoparticles

α–Fe_2O_3/MWCNT/AuNPs–α–Fe_2O_3 / multi walled carbon nanotubes / gold nanoparticles

GCE – glassy carbon electrode

MWCNT – multi walled carbon nanotubes

$K_3[Fe(CN)_6]$ – potassium ferricyanide

DD – distilled deionized

SEM – scanning electron microscopy

AFM– Atomic force microscopy

XRD – X-ray Diffractometer

PBS solution – phosphate buffer solution

$HAuCl_4$ – chloroauric acid

KNO_3 – Potassium nitrate

fcc – face-centered cubic

LSVs – linear sweep voltammograms

LOD – limit of detection

Abstract

The electrochemical behavior of riboflavin (RF) at a glassy carbon electrode modified with α-Fe_2O_3/MWCNT/AuNPs was investigated by cyclic voltammetry (CV) and square wave voltammetry (SWV). The redox behavior of the RF was examined in detail in phosphate buffer solution using variable scan rate cyclic voltammetry (V=20 mVs^{-1}−10 Vs^{-1}) and has been found to undergo a series of proton-coupled electron transfer reactions. Also, the interaction of RF with double stranded DNA (ds-DNA) based on the oxidation signal of guanine base was studied using SWV. Our sensor fabrication did not take into account the pretreatment procedure of the modified electrode before to immobilize the ds-DNA, which shows that our composite material has highly electroactive and more functional groups to interact with ds-DNA. The decrease in the intensity of the guanine oxidation signal after interaction with RF was found as an indicator signal for the sensitive determination of RF. These results additionally confirmed that this RF-ds-DNA interaction could be used for the sensitive and accurate detection of RF. The peak current on the modified electrode was linear over a range from 0.3μM to 0.6×10^{-8} M, with the detection limit of 6 nM (3σ/b). The analytical performance of this sensor was demonstrated in real samples with satisfactory recovery.

Keywords: riboflavin, ds-DNA drug, square wave voltammetry, nanodendrites, gold nanoparticles, real samples

1. Introduction

Riboflavin (RF) is an essential vitamin in human nutrition occurring in a wide variety of food products. In the body RF is transformed into two active coenzymes, flavin mononucleotide (FMN) and flavin adenine dinucleotide (FAD). RF is taken up by RF receptors, which are expressed as both soluble and membrane-bound isoforms [1]. Moreover, RF receptors contain one type of potential tumor biomarker for cancer targeted delivery of therapeutic agents and imaging molecules [2-3]. This biomarker is relatively new as a receptor considered for cancer targeting compared to other biomarker proteins [4-7]. Multiple Acyl-CoA dehydrogenation deficiency, an autosomal recessive disorder is well responsive to treatment with RF [8]. The combined RF and ultraviolet-A treatment has revealed to increase gene mutations by seven times compared to UV radiation exposure alone [9]. Also, the concentration of RF in urine influences to cause some problems. Therefore, the accurate determination of RF level has to be measured to treat the diseases. Various techniques have been used for determination of RF including chemiluminescence [10], high performance liquid chromatography coupled with fluorimetric [11] or ultraviolet [12], mass spectrometry [13], voltammetry [14], surface plasmon resonance [15], fluorescence [16], spectrophotometry [17]and electrochemical approach [18]. Among these techniques, the electrochemical method has received a lot of attention because of their high sensitivity, selectivity, inexpensive, highly sensitive, long-term reliable, reproducible and convenience.

Nucleic acids play an important role in the recognition and monitoring of many important compounds such as drugs [19–21]. Electrochemical analysis of ds-DNA–drug intercalation provides a rapid and low-cost method for the determination of drugs. Changes

in the DNA structure during intercalation with DNA binding molecules are identified by nucleic acid recognition layer. The investigation based on DNA interaction is indispensable in order to analyze the mechanism of many drug compounds and fabrication of new DNA biosensors. Based on these importance, the ds-DNA and RF interaction is investigated in the proposed fabrication of RF sensor.

Iron products have recently attracted a great deal of interest for its promising applications as catalysts, adsorbents, batteries, pigments, and so on [22-29]. In particular, α-Fe_2O_3 (hematite, Eg = 2.1 eV), the most researched polymorph, is believed to be a promising candidate to replace graphite because of its high theoretical capacity (1007 $mAhg^{-1}$), low cost, ease of fabrication and environmental friendliness [30–32]. However, during charge/discharge process, Fe_2O_3 suffers from crumbling, pulverization, consequent fast capacity fading and low conductivity [26–28]. Interestingly, such drawbacks can be overcome by the fabrication of hybrid Fe_2O_3 nanomaterial with CNT (porous structure and excellent electrical conductivity) as one of the most effective ways towards high-performance composite preparation. In this paper, we synthesis Fe_2O_3 nanodendrites, because the dendritic nanostructured materials have attracted significant attention due to their importance in crystallography research, wide applications in nanosensors [33] and microdevices [34] with high degree of structural anisotropy and highly active facets of their surface [35].

Zhou et al. [36] have prepared Fe_2O_3/CNT membrane as a high-performance anode for lithium ion batteries, exhibiting a discharge capacity of 801 $mAhg^{-1}$ after 90 cycles. The highly conducting CNT network in the composite not only facilitates electron transfer of Fe_2O_3, but also enhances the electrochemical activity and mechanical integrity of the electrode due to their large surface area, diffusion length and sufficient internal void space [38]. Furthermore, the CNT

architecture may serve as a structural buffering layer to cushion the internal strain by preventing the Fe_2O_3 nanostructures from being electrically isolated upon cycling [37, 39]. Also, it is observed that few efforts have been made to carry out reactions for various applications on Fe_2O_3 metal catalysts encapsulated/wrapped within nanotubes [40-43].

Gold nanoparticles (AuNPs) have been utilized in a variety of research fields owing to the efficient integration of the unique catalytic properties and the excellent surface/interface recognition ability contributed from the rational design of the surface chemistry [44]. The rational design of the surface chemistry of AuNPs enhances specific interactions between the receptors and analytes and, hence, makes the measurements highly selective and sensitive [45].

In this investigation we have described the use of an electrochemical procedure, to fabricate α–Fe_2O_3/MWCNT/AuNPs composite onto the surface of glassy carbon electrode (GCE) in order to challenge the determination of RF by SWV method (Scheme 1 and Scheme 2). Hence, the combination of this composite with unique properties may bring forth an unexpected and interesting catalytic performance in RF sensing.

Scheme 1 and Scheme 2

2. Experimental

2.1. Reagents

Double-stranded herring testes DNA with an average molecular weight ~50 kbps (base pairs), RF, MWCNT (99%), potassium ferricyanide $K_3[Fe(CN)_6]$ 98.5% and hexadecyl trimethyl ammonium bromide were purchased from Sigma Aldrich, India. All chemicals were of reagent grade quality and used as received without further purification. Reagent solutions were freshly prepared before use. Distilled deionized (DD) water was obtained by a Millipore water system and used throughout. Stock 1 mM solution of RF was prepared before use and protected against light. The stock DNA solution (0.06 g per 50 mL) was prepared by mixing a measured amount of DD water.

2.2 Instrumentation

The surface morphology of the samples was investigated by scanning electron microscopy (SEM, JEOL Ltd) and atomic force microscopy (AFM, Agilent 5500). The X-ray diffraction (X-RD) was performed on an X-ray Diffractometer System (Bruker Germany D8 Advance) with Cu Ka radiation (1.5418 Aº). Electrochemical signals were measured with a CHI 6005D electrochemical workstation (Austin, USA) using a GC working electrode (0.07 cm^2), an Ag/AgCl (3 M KCl) reference electrode and a platinum wire auxiliary electrode. The prepared phosphate buffer solution (PBS) (pH 7.2) was purged with nitrogen gas for 10 minutes prior to all the electrochemical experiments. All the measurements were carried out in PBS under nitrogen atmosphere at room temperature and acetate buffer (pH 4.8) containing 0.02 mol L^{-1} NaCl was also used to study the ds-DNA and RF interaction.

2.3 α-Fe_2O_3/MWCNT composite preparation

α-Fe_2O_3 nanodendrites doped with MWCNT were synthesized by a facile and environmental friendly hydrothermal method. The acid wash of MWCNT was done as reported in our previous paper [46]. The diameter of the MWCNT is given from the manufacturer of the company as 40 nm. In a typical synthesis, 0.02 M concentration of potassium ferricyanide $K_3[Fe(CN)_6]$ 98.5%, 5 mg hexadecyl trimethyl ammonium bromide and 2.5 mg of MWCNT were dissolved in 80 mL of DD water. After magnetic stirring for until completely dissolved, the solution was transferred to a teflon lined stainless steel autoclave (100 mL capacity) and then kept at 180º C for 24 h, after cooling naturally, the collected precipitate was harvested by centrifugation and washed thoroughly with water and ethanol before being dried at 100ºC for 12 h.

2.4 Fabrication of GCE modified with α–Fe_2O_3/MWCNT/AuNPs composite

Prior to surface modification, the bare GCE was polished with gamma alumina suspensions 1.0, 0.3 and 0.5 μM respectively. After that, the electrode was successively washed in ethanol and DD water for 15 minutes by ultrasonic method. The as prepared α–Fe_2O_3/MWCNT composite was dispersed in DD water (1 mL) and drop casted (10 μL) onto the GCE and air dried at room temperature for 1 h. The AuNPs were electro-deposited onto α–Fe_2O_3/MWCNT composite at a constant potential −100 mV for 300 s in 2 mM $HAuCl_4$ in 0.1 M KNO_3 solution according to our previous report [47].

2.5 Fabrication of α–Fe_2O_3/MWCNT/AuNPs/ds-DNA modified electrode

In this study, 10μL of ds-DNA was covalently immobilized by drop cast method on the α–Fe_2O_3/MWCNT/AuNPs modified electrode and dried it for 1 h at room temperature. Then the

surface of DNA immobilized electrode was washed with 5% sodium dodecyl sulfate in PBS solution to remove the unbound DNA.

2.6 Interaction between ds-DNA and RF at the ds-DNA modified electrode

The DNA-modified electrode was immersed in the electrolyte 0.2 M acetate buffer (pH 4.8) and a positive-going SWV (from +0.40 to +1.40 V) was performed. The oxidation signal of guanine was recorded. For understanding the interaction of RF with ds-DNA, the modified electrode was immersed into acetate buffer solution (pH 4.8) containing different concentrations of RF and their corresponding guanine peaks were recorded. The obtained curves before and after interactions between RF and ds-DNA were compared with each other.

3. Results and discussion

Figure 1

3.1 SEM analysis

The morphology of the nanostructured α–Fe_2O_3, MWCNT, α–Fe_2O_3/MWCNT and α–Fe_2O_3/MWCNT/AuNPs was characterized by SEM as shown in Fig.1. The surfactant assisted α–Fe_2O_3 exhibits uniform dendritic shaped nanostructures with well defined main trunk, branches and sub-branches as indicated in Fig. 1(A). Fig. 1(B) shows the individual MWCNT has smooth surface, typical tube morphology and randomly align to form a network structure, which is beneficial for accommodating the volume expansion and facilitates the electron transfer mechanism. It can be observed from Fig. 1(C) that the doped MWCNTs is seen on the surface of α–Fe_2O_3 dendrites as indicated by red circles; while the wall of the MWCNT not injured by the dendrites and also many crevices in the surface of MWCNTs, which are useful to increase the

contact area of electrode and electrolyte and this information is also supported by AFM image Fig.S3. Fig. 1(D) shows the image of AuNPs deposited on the surface of α–Fe_2O_3/MWCNT composite without agglomeration.

3.2 X-RD studies

Figure 2

The crystallographic structure of the hybrid material was analyzed by X-RD. In Fig.2(a), the micro pin dendrites of pure α–Fe_2O_3 which has the rhombohedral structure with the characteristic peaks at 2θ of 33.3, 35.6, 49.5, 54.1, 62.4 and 64.0 are indexed as (104), (110), (024), (116), (214) and (300) depicting high purity and crystallinity. It is noted from the JCPDS cards no: 33-0664 that well matched for iron oxide and no other hydroxide, maghemite, magnetite peaks are observed exhibiting the hematite phase. A weak broadening [Fig.2 (b)] diffraction peak at 26.3 is well indexed as the (002) reflection of graphite (JCPDF 75-2078). In the deeper context, the (002) peak corresponding to MWCNT undergoes a suppressed broadening in the Fe_2O_3/MWCNT composite mixture indicates the deformation of the graphite structure of MWCNT [Fig.2 (c)]. This exact kind of broadening at 26.3^o has been previously observed as reported by Vinod kumar et al as the reflection plane of MWCNT [48]. After the inclusion of gold particles in the Fe_2O_3/MWCNT composite the abrupt peak disappearance of (002) peak can be observed in Fig.2 (d) due to complete destruction of the graphite structure of MWCNT. Also, the subsequent decrease/increase in the (104) and (111) peak intensity can be seen respectively. While, the characteristics of (111) peak along with (220) and (311) clearly

attribute to the AuNPs single face-centered cubic (fcc) structure as Keqiang Ding et al has previously reported [49].

3.3 Cyclic Voltammetry studies of α–Fe_2O_3/ MWCNT/AuNPs modified GCE

Figure 3

We examined the modified electrode by CV in the presence of 100 μM of RF solution. It is clearly seen in 3(A) the waves 'a' and 'b' don't show clear peaks suggesting the kinetics are slow due to weak adsorption of RF. But the redox peaks of wave 'c' depicts the enhancement of RF adsorption in the MWCNT modified electrode while wave 'd' is the result of negatively charged/functionalized MWCNT with positive charges of α–Fe2O3 and this composite transfer more electrons in the RF solution. On the other hand, the AuNPs electrochemically deposited on the α–Fe_2O_3/MWCNT enhance the catalytic activity in RF and yield great intensity current as seen in the wave 'e'. Further, the redox behavior of cyclic voltammograms confirmed that two electron-two proton oxidation/reduction reaction in the electro catalysis reversible reduction of RF at the α–Fe_2O_3/MWCNT/AuNPs modified electrode and also proved an excellent stability along repetitive cycling of the potential.

The kinetics of electrode reaction in the presence of RF was investigated using CV by evaluating the effect of scan rate. CV at various scan rates obtained at α–Fe_2O_3/MWCNT/AuNPs GCE in nitrogen saturated PBS (pH 7.0) containing 100 μM of RF illustrate that the anodic and cathodic peak currents increase with the increase in the scan rate, which confirms that the oxidation is a reversible process as seen in Fig. 3B. Further, with the increase of scan rate, the

oxidation peak shifted to the positive direction and the reduction peak moved to the negative direction, and the peak-to-peak separation was increased. The inset of Fig.3B plot of the oxidation peak current against the square root of scan rate (2–100 mVs^{-1}) shows an excellent linear relationship indicating that the oxidation reaction of RF is diffusion controlled process, which is an ideal case for quantitative measurements. The reversible nature of Fe_2O_3/MWCNT/AuNPs modified electrode in $[Fe(CN)_6]^{3-/4-}$ solution was also studied and shown in Fig.S1.

Figure 4

3.4 CV study on different scan rate of modified electrode in 1µM RF

It can be clearly observed in Fig.4 two oxidation waves in the reverse direction and two reduction waves in the forward direction at lower scan rates. Also, it is noted that at slow scan rates, the wave 1 was small due to decomposition of RF species. As the scan rate increases, wave 1 becomes larger while wave 2 diminishes subsequently in magnitude. The change in relative size of waves 1 and 2 can be elucidated by the reduction process (wave 3, wave 4) forms the protonated anion which can then be voltammetrically oxidized (wave 2) when the scan direction is reversed. As the scan rate is increased, the protonation reaction of the initially formed radical anion is outrun; hence, wave 1 that is coupled with oxidation of the radical anion increases in magnitude [50].

The theoretical full width at half maximum (fwhm) for an ideal Nernstian two-electron transfer process is 45.3mV (90.6/n). The fwhm for a RF-modified electrode ranged from 60 to 100 mV, as reported in literature [51-52]. But small variations are generally attributed to the high

concentration of redox active species at the electrode /solvent interface [53]. The peak widening is caused by the separation of the flavin's single two-electron reduction wave into 2 weakly resolved waves. These waves occur from one-electron reduction of oxidized flavin to the semiquinone form and then another one-electron reduction to fully reduced dihydroflavin with different pH solutions [54]. This high concentration of flavins could modify activities at the electrode surface and develop interactions between immobilized flavins undergoing redox processes, thereby leading to broadened peaks [55].

Figure 5

3.5 Dependence of Ep on pH

The effect of pH on the redox potential of the covalently linked RF is similar to the solution characteristics of RF in that with an increase in pH the peak potential shifts to negative values [56]. It is observed from Fig.5 (A) the redox peak is observed at -354 mV at pH 3 ; it shifts to -369 mV at pH 4; -421 mV at pH 5; -443 mV at pH 6; and to -492 mV at pH 7 . It is found that peak potential shifts to more negative value of the applied potential when pH changes from 3 to 7 and concluded that the adsorbed RF molecule does not become deprotonated up to pH 7.0. As reported by Gortonlg et al., [57] the RF does not become deprotonated due to the following reasons: (1) the attachment may be strong enough to change the pKa of the molecules on the modified surface. (2) The molecules are well packed in such a manner that the acid groups are shielded and, hence, are not available for deprotonation.

3.6 Linear sweep voltammetric study of RF

Fig. 5B shows the linear sweep voltammograms (LSVs) obtained for RF in the concentration range of 10–100 μM at the α–Fe_2O_3/MWCNT/AuNPs modified electrode. The

oxidation current of RF increased with a slight right shift while the peak potential was almost remained unchanged with increasing the scan rate upon each increment of 10 μM. The oxidation currents had a linear relationship with the concentration of RF with a correlation coefficient of 0.99785 (inset of Fig. 5B).

Figure 6

3.7 Sensitivity of the modified electrode using SWV

Furthermore, SWV was performed to examine the sensitivity of the α–Fe_2O_3/MWCNT/AuNPs modified electrode towards the detection of RF. Fig.6 depicts the curves of the α–Fe_2O_3/MWCNT/AuNPs modified electrode in PBS (pH 7.0) for different concentration of RF recorded at the potential between -0.6 and -0.2 V at amplitude of 0.025 V and a step potential of 0.004 V. The SWV results show that the analyte RF is oxidized with well-defined and distinguishable sharp oxidation peaks. With an increase in the concentration of analyte, the anodic peak current increases significantly. The modified electrode shows excellent electrocatalytic activity towards RF oxidation, individually, in the PBS (pH 7). To verify the linear relationship between anodic peak currents and analyte concentration, calibration curves are constructed. The peak currents are found to increase linearly with increase in the concentration of RF in the electrochemical cell. A linear dynamic range from 0.3μM to 0.6×10^{-8} M at the α–Fe_2O_3/MWCNT/AuNPs modified electrode with a correlation coefficient of 0.9956 was obtained for RF. From the square wave voltammetry, the different concentration of riboflavin and their corresponding current values are noted from the Fig.6. These values are entered in the origin lab software and plotted. Using linear fit option, a straight line is obtained. In that line, the

parameters such as slope of the calibration curve (b) and standard deviation (σ) values are obtained. Then, these values are substituted in the formula 3σ/b, to get the limit of detection. The detection limit was found to be 6 nM (inset of Fig. 6). The distinguished separation of the oxidation peak currents and high sensitivity provide good opportunity for the precise determination of RF at α–Fe_2O_3/MWCNT/AuNPs/GCE.

3.8 Interaction of RF with ds-DNA at the modified electrode using SWV

Figure 7

Various pretreatment procedures have been adopted to achieve faster electron transfer rates and more reproducible results. Such pretreatments are believed to result in an increase of surface and other functional groups, which can then catalyze the oxidation/reduction of the analyte[59,60]. Normally pretreatment of modified electrode was carried out before immobilization of the ds-DNA, to activate electrode surface for the immobilization. It was also proved that the ds-DNA was not immobilized on the surface of modified electrode without pretreatment and activation of the surface. The reason for the low activity may result from the lack of functional groups on the surface [58]. But in the present work, we have immobilized the ds-DNA without any pretreatment of the modified electrode. This shows that our composite material (α–Fe_2O_3/MWCNT/AuNPs) has highly electroactive and more functional groups to interact with ds-DNA. Further, this combination of α–Fe_2O_3/MWCNT/AuNPs/ds-DNA is also effective in sensing with different concentration of RF.

The ds-DNA was attached onto Fe_2O_3/MWCNT/AuNPs through both physical and chemical interactions between the AuNP and functional groups of the nitrogenous bases in DNA. The

interaction of RF with the ds-DNA-modified electrode was studied by SWV analysis as shown in Fig.7. In Fig. 7(A) different concentration of RF were used to interact with the ds-DNA on the modified electrode. The redox behavior of ds-DNA immobilized exhibits one oxidation process of guanine (1.01 V) residue as shown in curve a. This is supported by earlier reports [61,62]. The curves b to j are the result of each addition of 10 μgmL^{-1} of RF upto 90 μgmL^{-1} . The change in the current of the oxidation signal of guanine was obtained before and after interaction with RF. It was found that the oxidation peak current decreased with a concomitant increase in RF concentration. Thus, the reason for the decrease of the oxidation signals of the guanine was attributed to the binding of RF with DNA. Further, the decrease could be explained as a possible damage/shield or destabilization of the structure of oxidizable group of guanine base of DNA while interact with RF. The results also showed that guanine oxidation currents decreased with increase in concentration of RF up to 90 μgmL^{-1} and then almost leveled off. This is due to the fact the modified electrode surface was saturated by RF at higher concentration.

Fig. 7(B) shows different concentration ds-DNA interaction with varying concentration of RF and we understand the following:

(i) As the RF concentration is increased from 10 to 50 μgmL^{-1} the oxidation peak current of ds-DNA decreases gradually and then maintain constant.

(ii) As the ds-DNA concentration is decreased ($1X10^{-1}$ M to $1X10^{-6}$ M), the peak guanine base current found decreased linearly without addition of RF. In each concentration of ds-DNA give the same results as in the case (i).

Thus we additionally confirm our proposed sensor also capable of sensing RF with different concentration of ds-DNA. These types of experiments are very important to determine DNA sites and rational design of new DNA-targeted molecules for the application in cancer

therapy. Our obtained results showed that ds-DNA-modified electrode might be used for the detection of RF interaction with the ds-DNA. The immobilization of ds-DNA on the α–Fe_2O_3/MWCNT/AuNPs modified electrode was also studied in $[Fe(CN)_6]^{3-/4-}$ solution as depicted in Fig.S2.

3.9 Selective determination of RF in the presence of interfering compounds using the α–Fe_2O_3/MWCNT/AuNPs modified electrode

The anti-interference ability test by SWV of the α–Fe_2O_3/ MWCNT/AuNPs electrode towards the detection of RF was evaluated in the presence of 10 fold L-dopa, serotonin, epineprine, cystamine, dopamine, tyrosine and 100-fold excess of K^+, Ca^{2+}, NO_3^-, NH_4^+, Cl^-. No remarkable change was observed for 10μ μM RF with the foreign species. Results summarized in Table S1 show that the present modified electrode is highly selective towards the determination of RF even in the presence of these interferents with a relative standard deviation of 4.85%.

3.10 The stability and reproducibility of the α–Fe_2O_3/ MWCNT/AuNPs electrode

As repeated electrochemical continuous cycling in 100 μM of RF solution has no effect on film stability and does not cause leaching of the adsorbed RF even after several hours, it could be concluded that RF is strongly adsorbed on the modified electrode surface. Also, contact of the modified electrode with air does not cause loss of electroactivity. The reason for this strong binding is believed due to the Π-Π interaction of aromatic ring as well as NH group of RF with AuNPs deposited on the modified electrode. To ascertain the reproducibility of the results, six different GCEs were modified with the α–Fe_2O_3/MWCNT/AuNPs and their response towards the oxidation of 1 μM RF was tested. The peak current obtained in the measurements of six independent electrodes showed a relative standard deviation of 3.75%, confirming that the results

are reproducible. The performance of the fabricated RF sensor is very much comparable to the literature values (Table S3). The comparative data suggests that the present sensor has good sensitivity over some reported RF sensors, the possible reason being that the ferromagnetic behavior of the α–Fe_2O_3 coupled with high surface area and good electrocatalytic activity of MWCNT and AuNPs deposited.

3.11 Determination of RF in real samples

- The applicability of the modified electrode for determination of RF was verified by analysis of real samples. The α–Fe_2O_3/MWCNT/AuNPs modified electrode was applied for RF determination in pharmaceutical and milk powder samples using SWV technique. The milk powder samples were prepared before sensor measurements as follows: Initially, milk powder was weighed, and then dissolved in hot distilled water; proteins present in it were precipitated out by drop wise addition of glacial acetic acid. The solution was then digested in a water bath for several minutes and filtered through filter paper. The pH of the diluted filtrate was adjusted with boric acid and orthophosphoric acid to pH 7.0 and then the determination of RF was performed using SWV. To eliminate the interferences of surface active substances and other disturbing compounds likely to be present in the analyzed material, the standard addition method has attracted much attention for the determination of RF in real samples. The standard addition method is often used for electroanalytical chemistry whereby the standard is added directly into the electrolytes of analyzed sample. The standard addition method is used to investigate changes of analytical signal with respect to the addition. In this work, the standard addition method is carried out as follows: The real samples (pharmaceutical and milk

powder samples) have particular concentration of riboflavin and we have initially measured their SWV response. Then known concentration of riboflavin will be added (3 or 4 addition) into the similar solution and measured the SWV response signal. Finally we have obtained a corresponding calibration of peak current against riboflavin concentration. From this plot we can identify how much riboflavin present in real samples. Here, we have initially 1.0 μM of riboflavin in PBS prepared and measured SWV response. Followed by higher concentration of Interfering species (such as Serotonin, Epineprine, Cystamine, Dopamine, Tyrosine, Fe, Mg, Ca, K, NO_3, NH_4 and Cl) were separately added into 1.0 μM of riboflavin in PBS solution and then measured the SWV response, to analyze the interfering compounds affect the oxidation of riboflavin or not. The results are summarized in the Table S2. No sample pretreatment was needed for our proposed method in the case of pharmaceuticals and beverages.

4. Conclusion

The voltammetric behavior of RF using the α–Fe_2O_3/MWCNT/AuNPs has been investigated and the analytical method for the determination of RF in the buffer solution and afterwards in real samples was discussed in the present paper. The ferromagnetic α–Fe_2O_3 enhanced the catalytic behavior as doped with MWCNT and further electron transfer mechanism increased by the electrochemical deposition AuNPs. The redox behavior of RF was used for its determination. SWV technique with optimized experimental conditions was applied for the determination of RF in buffer solution. The α–Fe_2O_3/MWCNT/AuNPs GCE was utilized to detect RF which resulted excellent performance in sensitivity, stability, selectivity and reproducibility. Also the proposed sensor effectively interacts with ds-DNA directing to sensibly

detect different concentration of RF. All these advantageous features can make the proposed sensor applicable in medical, food or other areas.

Acknowledgement

Wilson would like to acknowledge Alagappa University for abundant support to execute the work.

References:

1 H.B. White and A.H. Merrill, *Annu. Rev. Nutri*., 1988, **8**, 279.

2 A. A. Karande, L. Sridhar, K.S. Gopinath and P.R. Adiga, *Int. J. Cancer,* 2001, **95**, 277.

3 T. Johnson, A. Ouhtit, R. Gaur, A. Fernando, P. Schwarzenberger, J.Su and M.F. Ismail, *Front.Biosci., Landmark Ed*., 2009, **14**, 3634

4 A. R. Hilgenbrink and P.S. Low, *J. Pharm. Sci.,* 2005, **94**, 2135.

5 X. Montet, M. Funovics, K. Montet-Abou, R. Weissleder and L. Josephson, *J. Med. Chem*., 2006, **49**, 6087.

6 R. Shukla, T.P. Thomas, A. Desai, A. Kotlyar, S.J. Park, and J.R. Baker, *Nanotechnology* , 2008, **19**, 295102.

7 S. Raha, T. Paunesku and G. Woloschak, *Wiley Interdiscip. Rev. Nanomed. Nanobiotechnol*., 2010, **3**, 269.

8 K. J. Rikke E.Olsen, Simon S. Olpin, Brage H. Andresen and Zofia H. Miedzybrodzka, *Brain,* 2007, **130**, 2045.

9 A. Besaratinia, S.I. Kim, S.E. Bates and G.P. Pfeifer, *Proc. Natl. Acad. Sci. U.S.A.,* 2007, **104**, 5953.

10 C.X. Zhang and H.L. Qi, *Anal. Sci.,* 2002, **18,** 819.

11 P. Vinas, N. Balsalobre, C. Lopez-Erroz and M. Hernadez-Cordoba, *J. Agric. Food Chem.,* 2004, **52**, 1789.

12 L.A. Kozhanova, G.A. Fedorova, and G. I. J. Baram, *J. Anal. Chem.,* 2002, **57**, 40.

13 S.M. Mandal, M. Mandal, A.K. Ghosh and S. Dey, *Anal. Chim. Acta,* 2009, **640**,

110.

14 R.O. Kadara, B.G.D. Haggett and B.J. Birch, *J. Agric. Food Chem.*, 2006, **54**, 4921.

15 I. Caelen, A. Kalman and L. Wahlstrom, *Anal. Chem.,* 2004, **76,** 137.

16 E.J. Lorent-Martinez, J.F. Garcia-Reyes, P. Ortega-Barrales and A. Molina-Diaz, *Anal. Chim. Acta,* 2006, **555,** 128.

17 T. Perez-Ruiz, C. Martinez-Lazazo, V. Tomas and O. Val, *Analyst,* 1994, **119,** 1199.

18 S. Shahrokhian and E. Asadian, *J. Electro anal. Chem*., 2009, **636**, 40.

19 T. Gua and Y. Hasebe, *Biosens. and Bioelect.,* 2012, **33,** 222.

20 W. Liping, L. Lin and B. Ye, *J. of Pharm. and Biom. Analysis,* 2006, **42,** 625.

21 R. Sakandar, H. Nawaz, K. Akhtar, M.A. Ghauri and A.M. Khalid, *Biosens. and Bioelectr.,* 2007, **27,** 2471.

22 M.J. Katz, S.C. Riha, N.C. Jeong, A.B.F. Martinson, O.K, Farha and J.T. Hupp, *Coord. Chem. Rev.,* 2012, **256,** 2521.

23 F.Le Formal, N. Tetreault, M. Cornuz, T. Moehl, M Grätzel and K .Sivula, *Chem. Sci.,* 2011, **2,** 737.

24 A.P. Singh, A. Mettenbörger, P. Golus and S. Mathur, *Int. J. Hydrogen Energy,* 2012, **37,** 13983.

25 S. Agarwala, Z.H. Lim, E. Nicholson and G.W. Ho, *Nanoscale,* 2012, **4,** 194.

26 T.W. Hamann, *Dalton Trans.,* 2012, **41,** 7830.

27 E.Thimsen, F. Le Formal, M. Grätzel and S.C. Warren, *Nano Lett.,* 2010, **11,** 35.

28 T.Vincent, M. Gross, H. Dotan and A. Rothschild, *Int. J. Hydrogen Energy,* 2012, **37,** 8102.

29 N. T. Hahn, H. Ye, D.W Flaherty, A.J. Bard and C.B. Mullins, *ACS Nano,*2010, **4,** 1977.

30 C.Z. Wu, P. Yin, X. Zhu, C.Z. Ouyang, and Y.J. Xie, *Phys. Chem. B,* 2006,**110,** 17806.

31 S. Chaudhari and M. Srinivasan, *J. Mater. Chem.,* 2012**, 22,** 23049.

32 L. Zhang, H.B. Wu, S. Madhavi H.H. Hng and X.W. Lou, 2012, *J. Am. Chem. Soc.,* **134,** 17388.

33 R. Qiu XL Zhang XL, Qiao R, Li Y, Kim YI and Kang YS. *Chem. Mat.,*2007,**19,**4174.

34 Je SS, Harrison JC, Kozicki MN, Bakkaloglu B, Kiaei S, Chae *J. J. Micromech. Microeng.,* 2009,**19,** 8.

35 C. Wang, H. Daimon, T. Onodera, T. Koda and S. Sun, *Angew. Chem*., 2008, **120,** 3644.

36 G.Zhou, D. Wang, P. Hou, W. Li, N. Li and C. Liu, *J. Mater. Chem.,* 2012, 22, 17942.

37 W. M. Zhang, X. L. Wu, J. S. Hu, Y. G. Guo and L. J. Wan, *Adv. Funct. Mater.,* 2008, **18,** 3941.

38 X. W. Lou, L. A. Archer and Z. C. Yang, *Adv. Mater.,* 2008, **20,** 3987.

39 X. W. Lou, C. M. Li and L. A. Archer, *Adv. Mater.,* 2009, **21,** 2536.

40. Z. Wang, D. Luan S. Madhavi, Y. Hud and X. Wen Lou, *Energy Environ. Sci.,* 2012, **5,** 5252.

41 Zhihui Ai, Yunan Wang, Mi Xiao, Lizhi Zhang and Jianrong Qiu, *J. Phys. Chem. C* 2008, **112,** 9847.

42 Wei Chen, Xiulian Pan and Xinhe Bao, *J. Am. Chem. Soc.,* 2007, **129,** 7421.

43 Nan Yan, Xuhui Zhou, Yan Li, Fang Wang, Hao Zhong, Hui Wang and Qia wang Chen. *Sci. reports,* 2013, **3,** 3392.

44 N. L. Rosi and C. A. Mirkin, *Chem. Rev.,* 2005, **105,** 1547.

45 Y. Jiang, H. Zhao, N. Zhu, Y. Lin, P. Yu and L. Mao, *Angew.Chem*., 2008,**120,** 8729; *Angew. Chem. Int. Ed.,* 2008, **47,** 8601.

46 C. Sumathi, P. Muthukumaran, S. Radhakrishnan, J. Wilson and Ahmad Umar, *RSC Adv.,* 2014, **4,** 23050.

47 J. Wilson, S. Radhakrishnan, C.Sumathi and V. Dharuman, *Sensors and Actuators B*, 2012, **171,** 216.

48 Vinod Kumar, Gopal Nath, Ravinder. K. Kotnala, Preeti S. Saxena and Anchal Srivastava, *RSC Adv.,* 2013, **3,** 14634.

49 Keqiang Ding, Hongwei Yang, Yahui Wang and Zhanhu Guo. *Int. J. Electrochem. Sci.,* 2012, **7,**4663.

50 S.V. Tatwawadi, K.S.V. Santhanam and A. J. Bard, *J. Electroanal. Chem.,* 1968, **17,** 411.

51 L. Gorton and G**.** Johannsson, *J. Electroanal. Chem.,* 1980, **113***,*151.

52 A.J. Diaz, *J.Am. Chem. Soc.,* 1977, **99,** 5838.

53 A. P. Brown and F.C. Anson, *J. Electroanal. Chem.,* 1977,**83,**203.

54 G**.** Dryhurst, *Electrochem. of Bio. Mol.,* Academic Press: New York, San Francisco, London, 1977, **365.**

55 C.N. Durfor, B.A. Yenser and M. L. Bowers**,** *J. Electro. Ana. Chem.* 1988, **244**, 287.

56 Berchmans, Sheela, Ph.D. Thesis, Alagappa University, India,1992.

57 L. Gorton and G. Johannsson, *J. Electroanal. Chem.,* 1980, ***113,*** 151.

58 R.C. Engstrom, *Anal. Chem.,* 1982, **54,** 2310.

59 A.Ozcan and Y. Sahin , *Electroanalysis*, 2009, **21**, 2363.

60 A.Ozcan and Y. Sahin , *Biosens. Bioelectron*., 2010, **25**, 2497.

61 G. Dryhurst, *Anal. Chim. Acta,* 1971, **57,**137.

62 G. Dryhurst and P.J. Elving, *J. Electrochem. Soc.,* 1968**, 5,** 1014.

Figure Captions

Fig.1 SEM images of (A) α–Fe_2O_3 nanodendrites (B) MWCNT (C) α–Fe_2O_3/MWCNT (D) α–Fe_2O_3/MWCNT/AuNPs

Fig.2 X-RD patterns of (a) pristine α–Fe_2O_3 (b) MWCNT (c) α–Fe_2O_3/MWCNT (d) α–Fe_2O_3/ MWCNT/AuNPs

Fig.3 (A) CVs obtained for RF (100 μM) at the (a) bare (b) α–Fe_2O_3 (c) MWCNT (d) α–Fe_2O_3/MWCNT (e) α–Fe_2O_3/MWCNT/AuNPs modified electrode recorded in PBS (pH 7.0) at a scan rate of 50 mVs^{-1} at a potential between -1.0 and 0.2 V and (B) CV obtained for RF (100 μM) at the α–Fe_2O_3/MWCNT/AuNPs modified electrode at different scan rates (2–100 mVs^{-1}) in PBS (pH 7.0).

Fig.4 Variable scan rate CV recorded at the α–Fe_2O_3/MWCNT/AuNPs GCE of 100μM RF in PBS (pH 7)

Fig.5 (A) Plot of oxidation peak current and voltage of RF Vs.pH (B) LSVs obtained for RF in the concentrations ranging from 10 to 100 μM. RF was added in steps of 10 μM each at the α–Fe_2O_3/MWCNT/AuNPs modified electrode in PBS (pH 7.0).

Fig.6 SWVs of α–Fe_2O_3/MWCNT/AuNPs modified GC electrode in nitrogen saturated PBS (pH 7.0) RF was added from 300 nM to 60μM; amplitude 0.025 V and step potential 0.004 V. Inset shows the resulting calibration plot

Fig.7 (A) (a) α–Fe_2O_3/MWCNT/AuNPs/ds-DNA (b)10 (c) 20 (d) 30 (d) 40 (e) 50 (f) 60 (g) 70 (i) 80 (j) 90 μgmL^{-1} of RF addition in the 0.2 M acetate buffer (pH 4.8). (B): different concentration of ds-DNA immobilized on the modified electrode (a) $1X10^{-1}$ M of ds-DNA (b) $1X10^{-2}$ M of ds-DNA (c) $1X10^{-3}$ M of ds-DNA (d) $1X10^{-4}$ M of ds-DNA (e) $1X10^{-5}$ M of ds-DNA (f) $1X10^{-6}$ M of ds-DNA

Figures

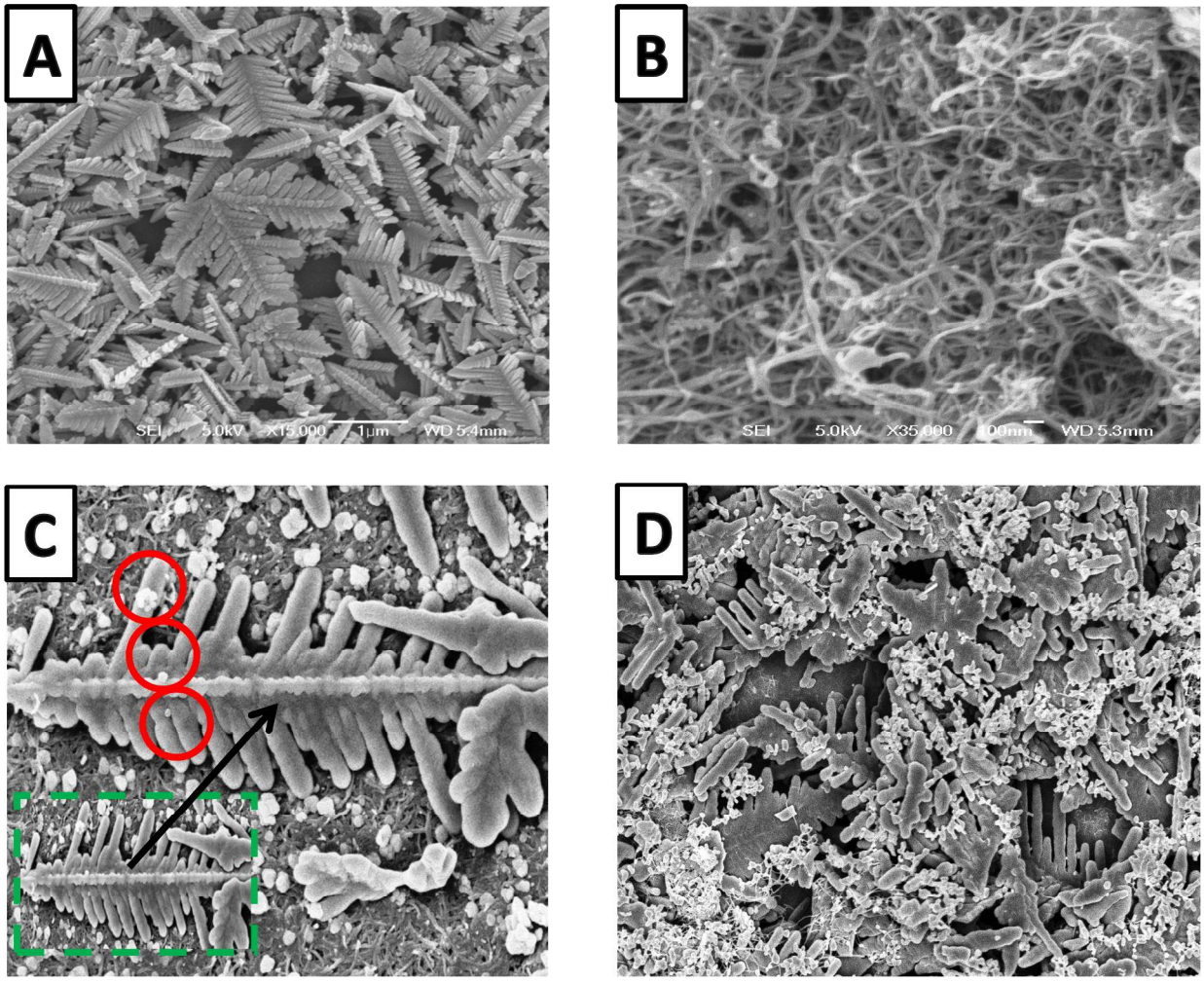

Fig.1

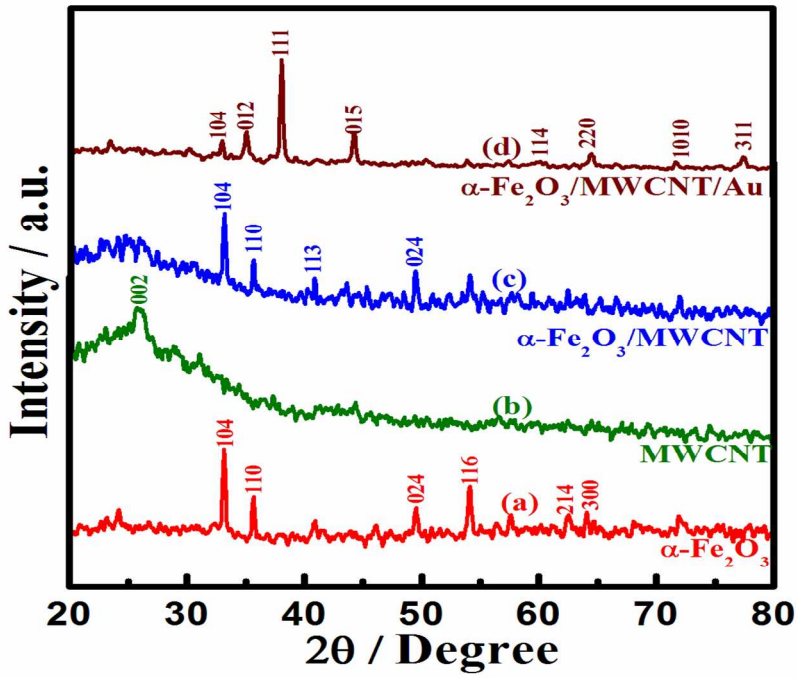

Fig.2

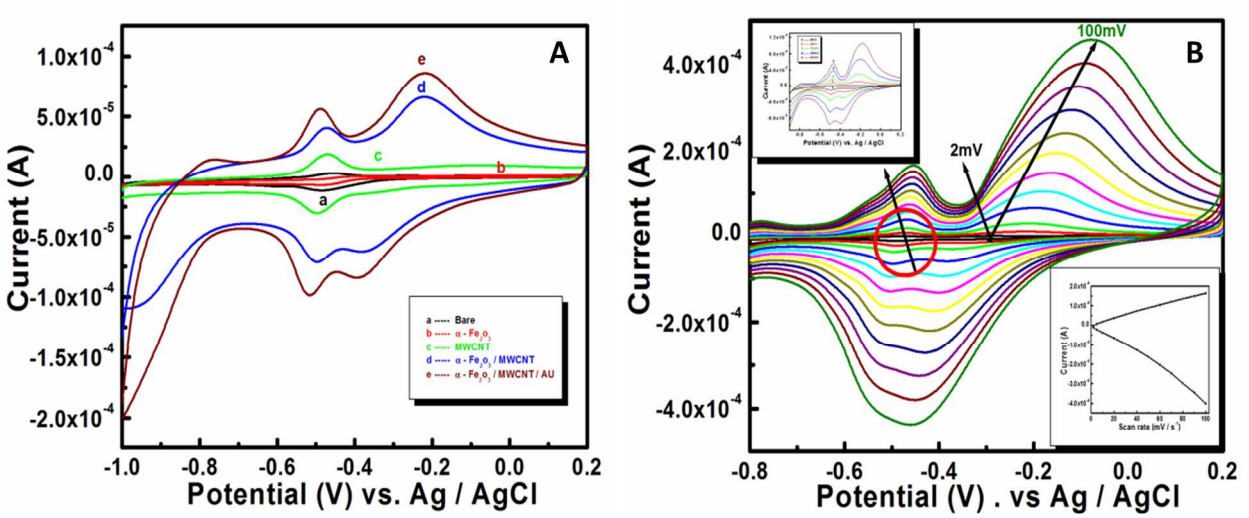

Fig.3

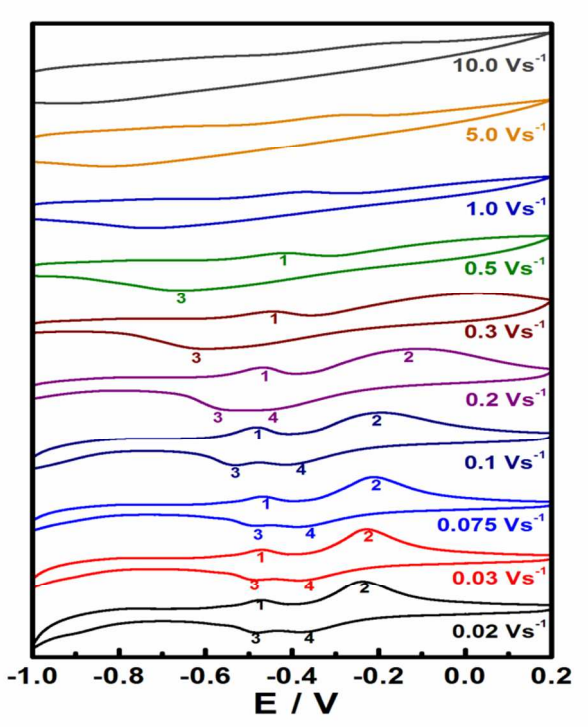

Fig.4

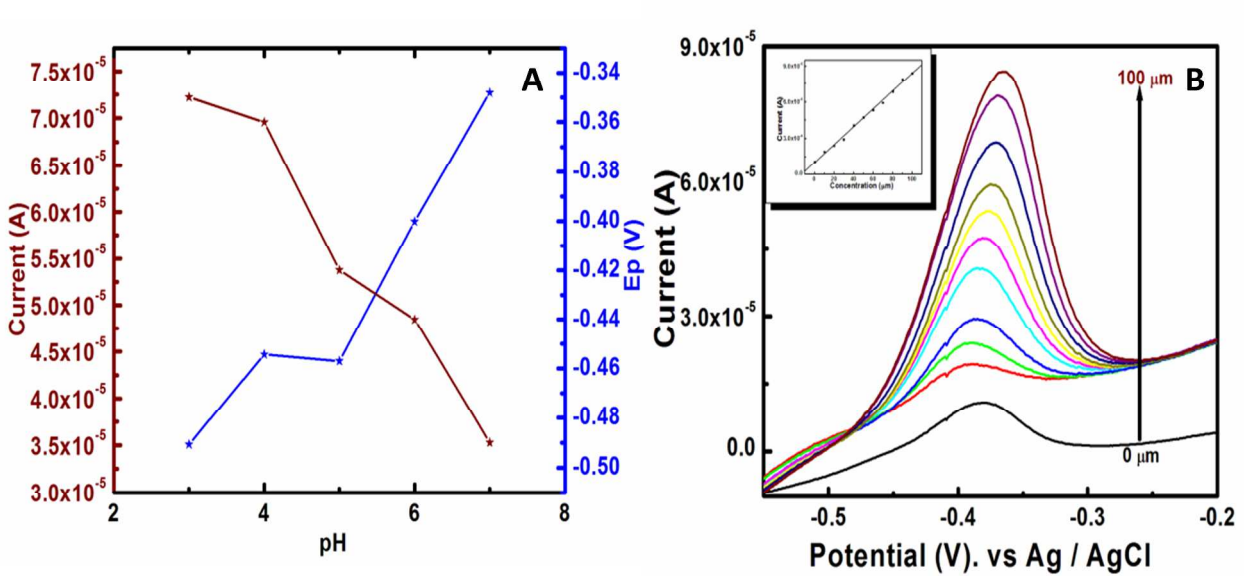

Fig.5

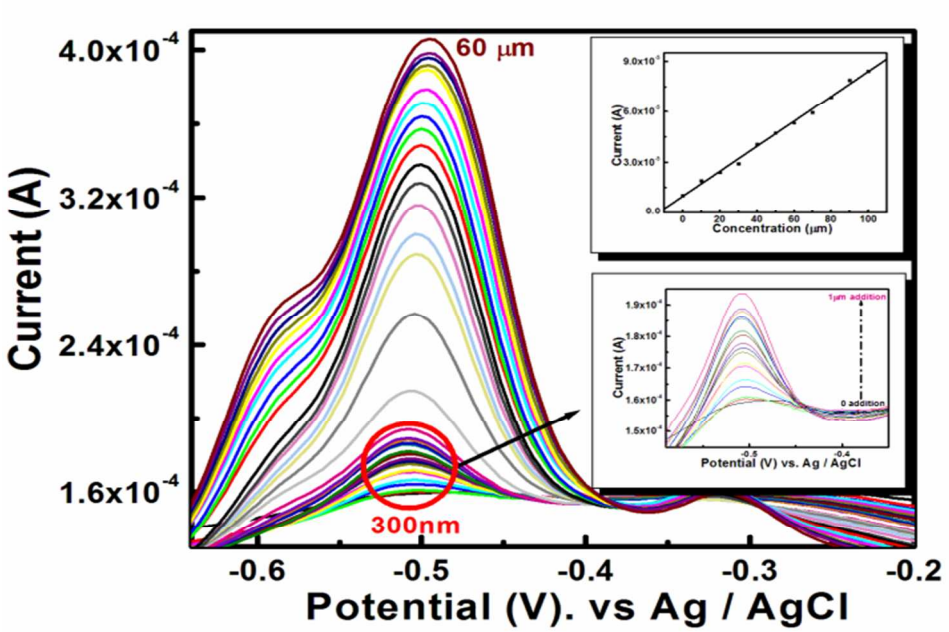

Fig.6

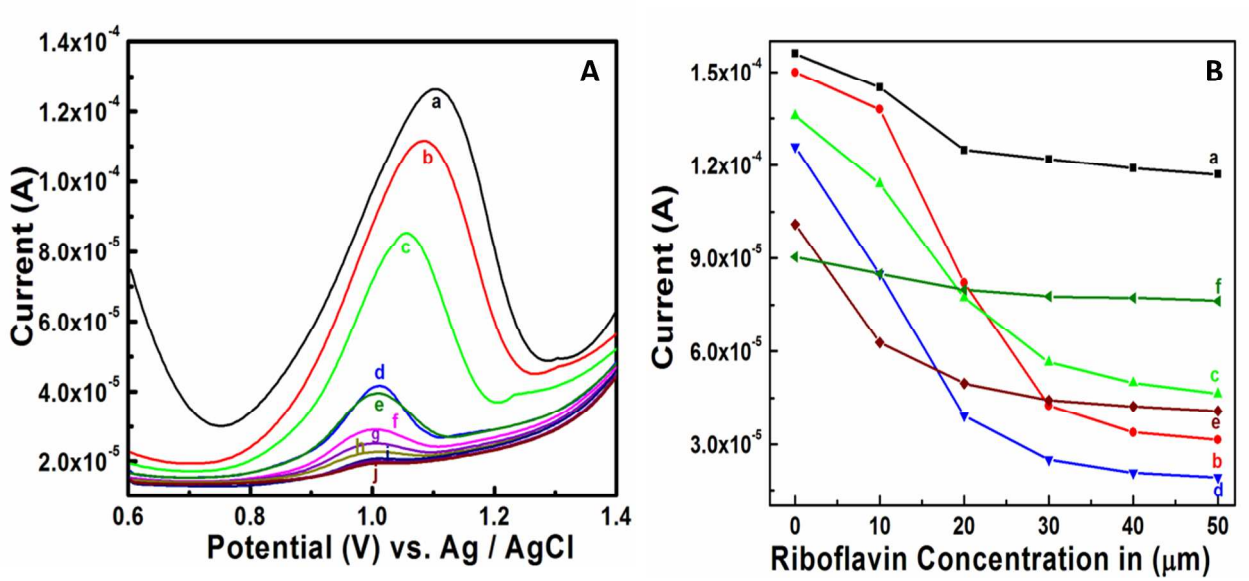

Fig.7